2019-01-01

Virtual source method simulation of progressive water waves

Al-Tameemi, O

Proceedings of the International Offshore and Polar Engineering Conference

Virtual Source Method Simulation of Progressive Water Waves

Omar Al-Tameemi [a,b], *David I. Graham* [a], *and Kurt Langfeld* [c]
[a] School of Computing, Electronics and Mathematics, Plymouth University, UK
[b] College of Science, Al-Nahrain University, Iraq
[c] Department of Mathematical Sciences, University of Liverpool, UK

ABSTRACT

The virtual source method (VSM) has been developed to simulate water waves based upon the solution of Laplace's equation for the velocity potential integral equations with full nonlinear surface conditions. The basis of the method is the use of specific Green's functions for a rectangular 'virtual domain' which is an extension of the physical domain. The solution variables are frequency components of the velocity potential at the upper virtual boundary and these are found by specifying appropriate conditions on the physical boundaries (i.e. wavemaker, walls and wave surfaces). The authors have shown that the model successfully simulates both linear and nonlinear standing waves and simple sloshing problems and is more effective and efficient than simple boundary element methods for these problems. In this paper, we develop the VSM to generate nonlinear progressive waves in a numerical wave tank. In order to remove the transmitted energy of the waves and so reduce the reflection from the right wall of the tank, an artificial damping term is added to the free surface boundary condition. The VSM results are compared with those from both second order Stokes theory and from a boundary element method (BEM).

KEY WORDS: Numerical wave tank (NWT), boundary integral equation, progressive waves.

INTRODUCTION

The numerical simulation of nonlinear water waves using the potential flow studies has been started in the 1970's. Longuet-Higgins and Cokelet (1976) were the first to simulate an asymmetric overturning deep water wave. They used a conformal mapping approach with space periodic boundary conditions and an artificial pressure distribution to enforce the breaking. Since then, many researchers have taken up the topic of nonlinear wave simulation, often in combination with wave-body interaction. Kim et al. (1999) reviewed the research on the development of numerical wave tanks (NWT's). More recently, a review on the topic of numerical wave modelling is given by Thomas and Dwarakish (2015). Most numerical methods for potential flow wave simulation are based on the mixed Eulerian-Lagrangian method to separate the elliptic boundary value problems (BVP) from the dynamic equations at the free surface. The vast majority of available numerical schemes that simulate free surface potential flow, approximate the BVP using a Boundary Integral (BI) formulation. Recently, Langfeld et al. (2016) introduced the virtual source method (VSM) for solving free-surface potential flow problems and applied it to simulate standing waves in 2D and 3D. Al-Tameemi et al (2018) illustrated the the energy and volume conservation of the VSM method for nonlinear standing wave simulation. In this paper we develop the VSM to simulate nonlinear progressive waves in a numerical wave tank. The results are compared with second order Stokes wave theory as well as boundary element method (BEM) numerical results.

GOVERNING EQUATIONS AND TANK GEOMETRY

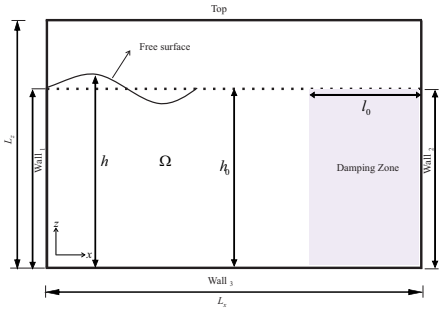

Fig. 1 Wave tank geometry.

An ideal fluid is assumed so that the fluid velocity can be described by the gradient of velocity potential ϕ. The simulation of waves generated by in a rectangular tank is undertaken in this section. The numerical wave tank considered here is illustrated in figure 1 which shows the wave propagation generated from the boundary condition on the left hand side. Also, an artificial damping zone is placed at the right side of the computational domain in order to absorb the waves approaching the far-right wall. A Cartesian coordinate system is chosen such that $z = 0$ corresponds to the calm water level and z is positive upwards. Then the governing equation of the velocity potential in the fluid domain Ω is Laplace's equation,

$$\nabla^2\phi = \frac{\partial^2\phi}{\partial x^2} + \frac{\partial^2\phi}{\partial z^2} = 0. \tag{1}$$

On the free surface, the kinematic free surface boundary condition is defined as,

$$\frac{\partial\eta}{\partial t} = \frac{\partial\phi}{\partial z} + \frac{\partial\phi}{\partial x}\frac{\partial\eta}{\partial x} \qquad \text{on } z = \eta, \tag{2}$$

while the dynamic boundary condition is defined by the following equation.

$$\frac{\partial\phi}{\partial t} = -g\eta - \frac{1}{2}|\nabla\phi|^2 \qquad \text{on } z = \eta. \tag{3}$$

To satisfy the impermeability condition (no-flux condition), the normal velocity is set to be zero at the stationary walls.

$$\frac{\partial\phi}{\partial n} = 0 \qquad \text{on Wall}_2 \text{ and Wall}_3. \tag{4}$$

Inlet boundary condition

There are two possible methods to set the inlet boundary condition, displayed as wall$_1$ in figure 1, (i) the creation of a piston-type wave maker, as is used in physical wave tanks or (ii) the use of a moving boundary condition. In this paper, a moving boundary condition was implemented by feeding the left boundary wall$_1$ by a horizontal velocity component.

Damping zone

In order to remove the transmitted energy of the waves and so to reduce the reflection from wall$_2$ shown in figure 1, the artificial damping term presented in Cointe (1990) is added to the free surface boundary condition as follows:

$$\frac{\partial\eta}{\partial t} = \frac{\partial\phi}{\partial z} + \frac{\partial\phi}{\partial x}\frac{\partial\eta}{\partial x} - \nu(x)z \qquad \text{on } z = \eta, \tag{5}$$

$$\frac{\partial\phi}{\partial t} = -g\eta - \frac{1}{2}|\nabla\phi|^2 - \nu(x)\phi \qquad \text{on } z = \eta, \tag{6}$$

in which $\nu(x)$ is the adjustable attenuation coefficient inside the artificial damping zone. This coefficient is defined to be a function of the position x and damping zone length l_0 as:

$$\nu(x) = \begin{cases} 0 & \text{for } x \le x_0 \\ \alpha\omega\left(\frac{x-x_0}{l_0}\right)^2 & \text{for } x > x_0 \end{cases} \tag{7}$$

in which x_0 is the position at which the damping zone will start to interact while α is the damping factor and l_0 is the damping zone length.

THE VIRTUAL SOURCE METHOD

Langfeld et al. (2016) presented the virtual source method (VSM) for simulation of standing waves by solving to Laplace's equation (1) for the problem expressed in figure 2.

According to Langfeld et al., (2016), the velocity potential can be expressed analytically by the following sum:

$$\phi_A(\mathbf{x}, t) = \sum_{n\in\mathbb{N}} \sigma_n(t)\cos(k_n x) F\left(\kappa n,\ \frac{z}{L_z}\right), \tag{8}$$

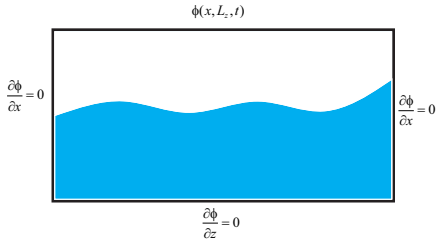

Fig. 2 Boundary conditions of Standing wave Scenario (A).

where $\sigma_n(t)$ is the n^{th} component of the Fourier cosine transform of the velocity potential along the top boundary, $k_n = \frac{\pi}{L_x}n$ and

$$F(k, z) = \sum_{\nu=0}^{\infty}(-1)^{\nu}\left[\mathrm{e}^{-\pi k(2\nu+1+z)} + \mathrm{e}^{-\pi k(2\nu+1-z)}\right], \quad k > 0. \tag{9}$$

The function F consists of an alternating sum with rapidly vanishing terms. It can be therefore numerically evaluated in a rapid and reliable way.

In order to generate a progressive wave, consider the scenario B which is the case of an inlet at the left hand side of the wave tank with a time dependent inlet velocity $u_B(z, t)$ shown in figure 3.

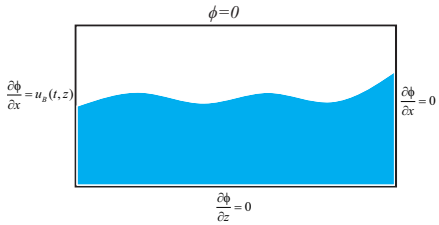

Fig. 3 Boundary conditions of inlet velocity Scenario (B).

The solution $\phi_B(x, z, t)$ has three homogeneous boundary conditions hence the separation of variables for the current set of boundary conditions suggests:

$$\phi_B(x, z, t) = \sum_{n\in\mathbb{N}} a_n(t)\ \cosh\Big(q_n(x - L_x)\Big)\ \cos(q_n z)\ , \quad q_n = (2n-1)\,\frac{\pi}{2L_z}\ . \tag{10}$$

We now in the position to express the coefficients a_n in terms of the inlet velocity profile $u_B(z, t)$:

$$u_B(z, t) \ = \ \frac{\partial\phi_B}{\partial x}\Big|_{x=0} \ = \ -\sum_{n\in\mathbb{N}} a_n(t)\ q_n\ \sinh\Big(q_n L_x\Big)\ \cos(q_n z)\ . \tag{11}$$

The a_n emerge after inverse Fourier transform. There is already an interesting observation: the latter equation might not have a solution. In this case, the problem is *ill-posed*. Note that the homogeneous velocity profile $u_B(t)$ falls into the class of ill-posed problems. From (11), it is clear that the profiles must satisfy $u_B(z = L_z, t) = 0$. Let us choose a mildly z-dependent profile function:

$$u_B(z, t) \ = \ u_{B0}(t)\ \cos(q_1 z) \ = \ u_{B0}(t)\ \cos\Big(\frac{\pi\, z}{2L_z}\Big)\ .$$

In this case, only a_1 is different from zero:

$$a_1 \;=\; -\frac{u_{B0}(t)}{q_1\,\sinh(q_1 L_x)}\;. \tag{12}$$

Altogether, the particular solution is:

$$\phi_B(x,z,t) \;=\; -\frac{u_{B0}(t)}{q_1\,\sinh(q_1 L_x)}\;\cosh\Big(q_1(x-L_x)\Big)\;\cos(q_1 z)\;. \tag{13}$$

The solution with the desired inlet boundary conditions is then given by

$$\phi(x,z,t) \;=\; \phi_A(x,z,t) \;+\; \phi_B(x,z,t)\;. \tag{14}$$

Numerical Implementation of the VSM

To compute the velocity potential and free surface components, the infinite sum (8) is replaced by a finite sum with a finite frequency components N_c as:

$$\phi_A(\mathbf{x},t) \approx \sum_{n=1}^{N_c} \sigma_n(t)\cos(k_n x) F\left(\kappa n,\;\frac{z}{L_z}\right), \tag{15}$$

Hence,

$$\begin{aligned}\phi(\mathbf{x},t) \approx &\sum_{n=1}^{N_c} \sigma_n(t)\cos(k_n x) F\left(\kappa n,\frac{z}{L_z}\right)\\ &-\frac{u_{B0}(t)}{q_1\,\sinh(q_1 L_x)}\;\cosh(q_1(x-L_x))\;\cos(q_1 z),\end{aligned} \tag{16}$$

From equation (15) , the velocity components can be found analytically at any point in space and time (mesh-free),

$$\nabla\phi_A(\mathbf{x},t) \approx \sum_{n=1}^{N_c} \sigma_n(t)\nabla\left[\cos(k_n x) F\left(\kappa n,\;\frac{z}{L_z}\right)\right]. \tag{17}$$

Then,

$$\begin{aligned}u(\mathbf{x},t) \approx &-\sum_{n=1}^{N_c} \sigma_n(t)\,k_n\cos(k_n x) F\left(\kappa n,\;\frac{z}{L_z}\right),\\ &-\frac{u_{B0}(t)}{\sinh(q_1 L_x)}\;\sinh(q_1(x-L_x))\;\cos(q_1 z),\end{aligned} \tag{18}$$

$$\begin{aligned}v(\mathbf{x},t) \approx &\sum_{n=1}^{N_c} \sigma_n(t)\;\cos(k_n x)\,\frac{\partial F}{\partial z}\left(\kappa n,\;\frac{z}{L_z}\right)\\ &+\frac{u_{B0}(t)}{\sinh(q_1 L_x)}\;\cosh(q_1(x-L_x))\;\sin(q_1 z).\end{aligned} \tag{19}$$

Now, Bernoulli equation (3) can be written as:

$$\frac{\partial\phi}{\partial t} = -gz - \frac{1}{2}\left[u^2+v^2\right] = B\left(\overline{\mathbf{x}},\eta(x,t),\sigma_n(t)\right) \qquad \text{on } z=\eta. \tag{20}$$

Hence,

$$\begin{aligned}\sum_{n=1}^{N_c}\dot{\sigma_n}(t)\cos(k_n x)F(\kappa n,z) = &\frac{\dot{u_{B0}}(t)}{q\,\sinh(qL_x)}\;\cosh(q(x-L_x))\;\cos(qz)\\ &+B(\mathbf{x},\eta(\mathbf{x},t),\sigma_n(t)),\quad q=\frac{\pi}{2L_y}.\end{aligned} \tag{21}$$

in order to calculate $\frac{d\sigma_n(t)}{dt}$, choose a set of resolution points: $N_x > N_c$, then:

$$\begin{aligned}\sum_{n=1}^{N_c}\dot{\sigma_n}(t)\cos(k_n x_i)F(\kappa n,z) = &\frac{\dot{u_{B0}}(t)}{q\,\sinh(qL_x)}\;\cosh(q(x_i-L_x))\;\cos(qz)\\ &+B(\mathbf{x_i},\eta(\mathbf{x_i},t),\sigma_n(t)),\quad i=1,...,N_x.\end{aligned} \tag{22}$$

The last two equations produces an overdetermined linear system to compute the time derivative of $\sigma_n(t)$. In this paper, we used the least squares to solve the above system then we used Runge-Kutta 4 integration to find $\sigma_n(t)$. However, Runge-Kutta integration need to compute the time derivative $d\eta/dt$ as the kinematic boundary condition (2) on the free surface where $\frac{\partial\tilde{h}}{\partial\tilde{x}}$ can be approximated by using the central finite difference scheme as follows:

$$\frac{\partial h}{\partial x} = \frac{h_{i+1}-h_{i-1}}{x_{i+1}-x_{i-1}} \tag{23}$$

with appropriate first-order backward or forward differences at $x=0$, $x=L_x$. Note that the elevation at the paddle/inlet at x=0 is not specified as a boundary condition but is found as part of the numerical solution.

Sequence of the Solution Procedure

For VSM, the sequence of solution can be summarised as:

1. Define the tank lengths, number of frequency components N_c and resolution points N_x.
2. Initialize the free surface profile.
3. Define the linear system (22) and solve it by using least squares.
4. Use Runge-Kutta 4 integration to find $\sigma_n(t)$ and finite difference to find $\frac{\partial h}{\partial x}$
5. Advance the solution in time by repeating the procedure (step 3-4) at every time step up to the final step.

NUMERICAL RESULTS AND DISCUSSION

We test our VSM formulation for a progressive waves scenario using two different test cases. In test case 1, we generate progressive waves in a numerical wave tank using second order Stokes solution as inlet boundary condition with and without absorption zone, while in test case 2, we compare our model with experimental data measured by Gao (2003).

Test case 1

A numerical wave tank is set with length 6m and initial water depth $h=0.5$m to generate water waves with different amplitudes for a time period $T=1$s and the wave number is calculated from the dispersion relation $\omega^2 = gk\tanh(kh)$. The damping zone conditions (5) and (6) with a length of two wavelengths and $\alpha=2$ is used in order to absorb the incoming wave energy which is reflected from the right boundary.

At the beginning of the computation, a ramp function is used to gradually build up the amplitude of the boundary velocity at the inlet boundary which leads to a more stable solution. For the current case, the ramp function given in equation (24) is used and time range is set to be 2 wave periods.

$$r(t) = \begin{cases} 1 & \text{for } t > 2T \\ \frac{1}{2}\left[1-\cos\left(\pi\frac{t}{2T}\right)\right] & \text{for } t \le 2T \end{cases} \tag{24}$$

Figure 4 compares the time history of the free surface elevation at the point $x=3m$ for 30 wave periods and two different wave heights $H=0.005m$ and $H=0.05m$ for the current VSM scheme and the converged boundary elements scheme (BEM) presented in Al-Tameemi et al. (2018). The time step is fixed at $\Delta t/T = 1/400$ and the number of

resolution points N_x for VSM and boundary elements along the free surface for BEM is fixed at 100 and the number of source points N_c for the VSM was set equal to 15. It can be seen for small wave steepness that the simulation results agree well with the second order Stokes solution . It can be noticed that for high wave steepness, nonlinear effects decrease trough depths compared with crest heights. However, the nonlinearity does not affect the frequency.

Figure 5 shows the numerical results of the free surface profiles at $t = 25T$. It can be noticed that there is a good agreement between the VSM and the second order solution. Moreover, it seems that the VSM scheme is more accurate than the BEM scheme for both small and large wave heights.

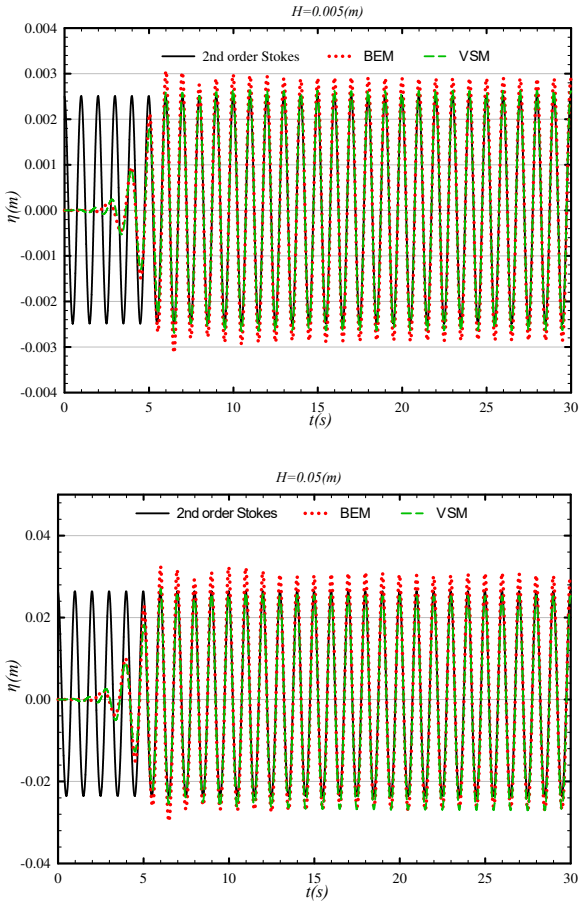

Fig. 4 Time history of water elevation at $x = 3m$ for $h = 0.5m$ and different wave heights.

To assess the stability of VSM, we run the simulation for 100 wave periods. Figure 6 gives the time history of the free surface elevation at the point $x = 3m$ for 100 wave periods. It can be seen that the scheme is stable even for large time step (100 time steps per period) and this is agrees with the observations of Al-Tameemi et al. (2018) for the standing wave case.

Figure 7 shows the free surface profiles of the waves over the full length of the tank after 80 wave periods. It is clear that the VSM result is consistent with the second order Stokes wave profile regarding of peaks but the trough depths are slightly under-predicted.

In order to investigate resonance phenomenon, we run the simulation with a hard boundary condition at the right end of the tank, i.e. (without absorption zone). Figure 8 shows the time history of the free surface elevation at the location $x = 3.0m$. It can be noticed that there is a steady increase in the wave height without changing the frequency for the small

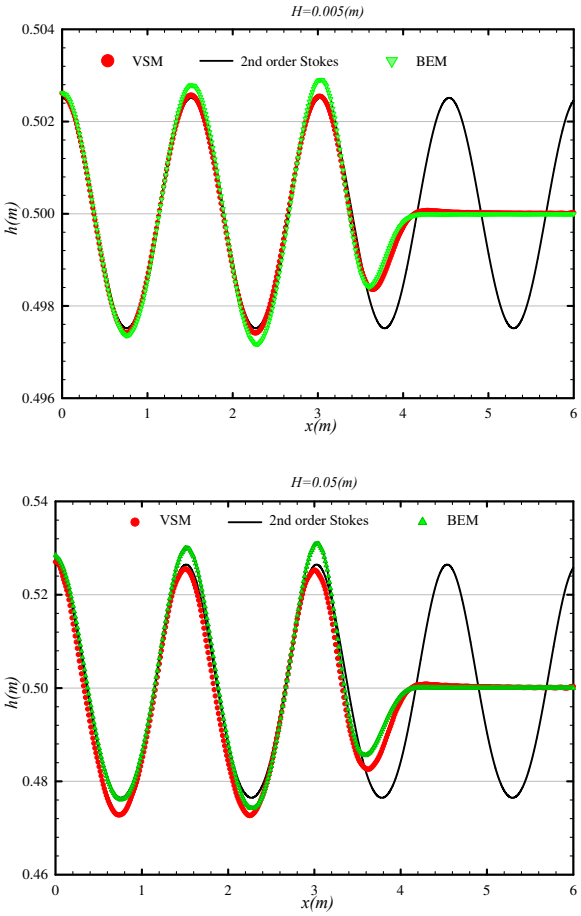

Fig. 5 Free surface shape at t=25 periods.

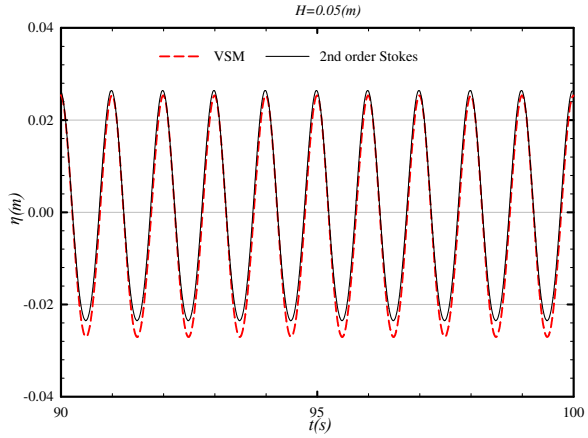

Fig. 6 Time history of water elevation at $x = 3m$ for $h = 0.5m$ and $H = 0.05m$.

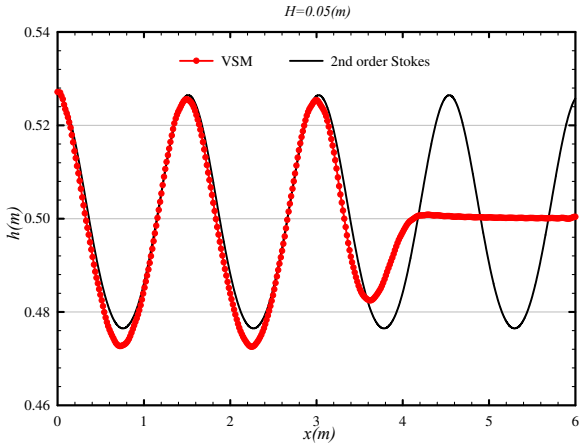

Fig. 7 Free surface shape at t=80 periods.

amplitude.This steady increase is due to continual re-reflection from the walls at each end of the wave tank. It can also be seen that there is a frequency interference after a certain number of periods in the high amplitude case.

Test case 2

In order to validate the present VSM scheme for more cases, the experiment conducted by Gao (2003) to investigate wave generation in a a physical tank is reproduced by the present scheme. Gao (2003) used an 8.85 m long wave flume with a still water depth of 0.28 m to generate regular waves by using a piston type wavemaker. The numerical investigations of this experiment have been reproduced by Qian et al. (2006) and Bai et al. (2010).

Gao (2003) used a piston type wavemaker with maximum displacement equal to 50 mm to generate regular waves of time period ($T = 1s$). Hughes (1993) derived the following relationship as a the first-order solution of a piston-type wave maker,

$$\frac{H}{S_0} = \frac{4\sinh^2(kh)}{\sinh(2kh) + 2kh}, \tag{25}$$

where S_0 is the stroke of the wavemaker.

We used the relationship (25) in order to approximate the wave amplitude and then define horizontal component of the velocity from second order Stokes theory at the inlet boundary condition. A linear ramp function is superposed from $t = 0$ to $t = T$. A total of 10 seconds was simulated to compare with the available experimental data as well as the BEM simulation.

In figures 9-11, the free surface elevations at the three different gauges above are compared with the corresponding experimental results. The figure shows a slight phase shift in the numerical results of the BEM scheme especially in gauge 2 and gauge 3 and this was also seen in the results of Qian et al. (2006) and Bai et al. (2010). In the VSM scheme, it can be seen that there is an excellent agreement between the numerical results and experimental results regarding the wave phase, crest heights and trough depths.

STEEP WAVES SIMULATION

In order to test the method for a high steepness waves, we run the scheme to generate progressive shallow water waves of 100m wavelength and 5m

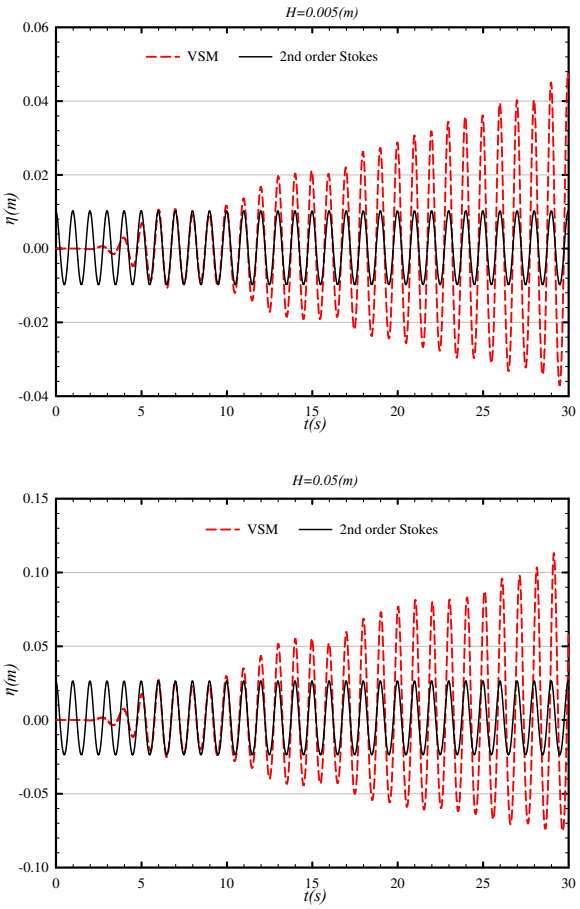

Fig. 8 Time history of water elevation at $x = 3m$ for $h = 0.5m$ and different wave heights.

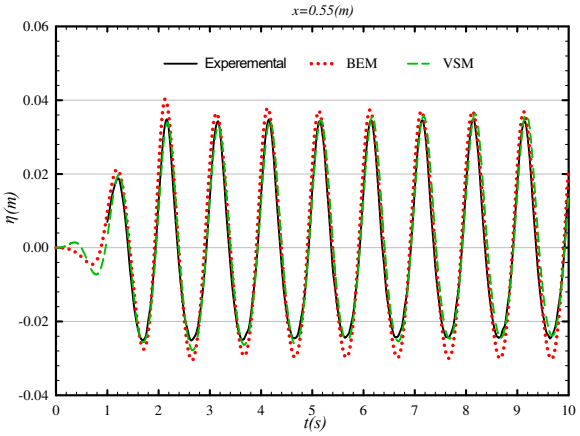

Fig. 9 Comparison between the experimental results of Gao (2003), BEM scheme and present VSM scheme for the free surface elevation at $x = 0.55m$..

wave amplitude where the initial water depth is chosen to be 15m. The

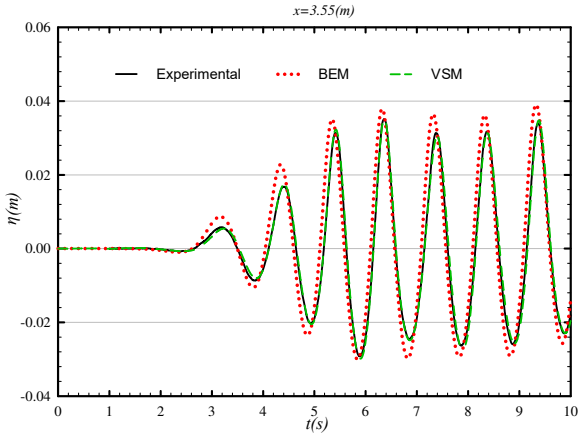

Fig. 10 Comparison between the experimental results of Gao (2003), BEM scheme and present VSM scheme for the free surface elevation at $x = 3.55m$.

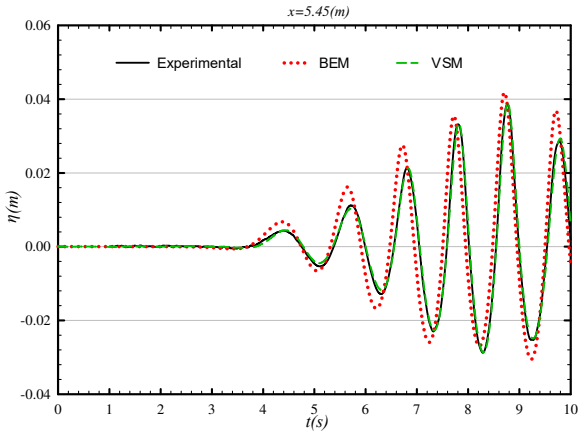

Fig. 11 Comparison between the experimental results of Gao (2003), BEM scheme and present VSM scheme for the free surface elevation at $x = 5.45m$.

numerical wave tank length is fixed at 5 wavelengths and the virtual top boundary is fixed at $L_y = 60m$. The simulation is run with 15 source points N_c and 60 resolution points N_x.

Figure 12 shows the time history of the water height at the middle of the tank. It can be seen that the method can successfully generated progressive waves for several periods and it seems that the (linear) dispersion relation $\omega^2 = gk\tanh(kh)$ remains valid. However, nonliearity is apparent in the non-regularity of the generated wave amplitudes.

CONCLUSIONS

In this paper, we have developed the Virtual Source Method (VSM) to simulate progressive waves in a numerical wave tank. The scheme has been validated by application to two test cases. In the first case, we simulate progressive waves with small and high amplitudes, with and without a damping zone. The results agreed with the second order Stokes and the BEM solutions. We have noticed resonance phenomenon when

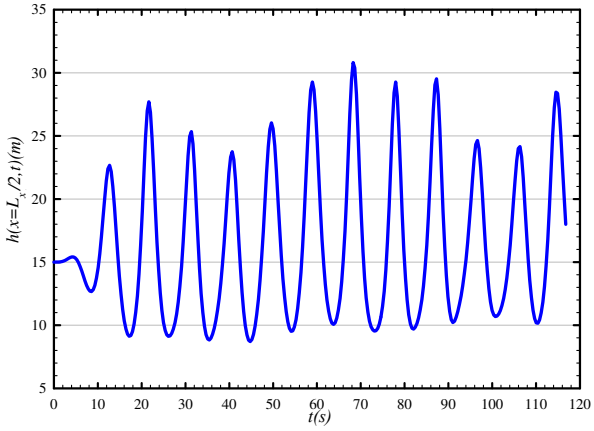

Fig. 12 Time history of water height at $x = 200$ for $h = 15$ and $H = 10$.

run the simulation without an absorption zone. The simulation has been run for 100 periods in order to check the stability and we observed that the scheme is stable even with a large time step. In the second test case, we compared our simulation results with the experiment conducted by Gao (2003). It was found that there was a excellent agreement with the experimental results in comparison with the solutions obtained by the other numerical schemes. Finally, in the of simulation high-amplitude progressive waves, nonlinear effects beyond second-order Stokes theory can easily be identified. Future work will include development of the method to simulate wave-structure interactions.

REFERENCES

Al-Tameemi, O, Graham, DI, and Langfeld, (2018). "Accuracy and Stability of Virtual Source Method for Numerical Simulations of Nonlinear Water Waves," Proc 28th Int Offshore and Polar Eng Conf, Sapporo, Japan, 10-15 June, 2018.

Bai, W., Mingham, C. G., Causon, D. M. and Qian, L. (2010), 'Finite volume simulation of viscous free surface waves using the cartesian cut cell approach', International Journal for Numerical Methods in Fluids 63(1), 69–95.

Cointe, R., (1990). Numerical simulation of a wave channel. Engineering Analysis with Boundary Elements, 7(4), pp.167-177.

Gao, F. (2003), An efficient finite element technique for free surface flow, PhD thesis, University of Brighton.

Hughes, S. A. (1993), Physical models and laboratory techniques in coastal engineering, Vol. 7, World Scientific.

Kim, C.H., Clement, A.H. and Tanizawa, K., 1999. Recent research and development of numerical wave tanks-a review. International Journal of Offshore and Polar Engineering, 9(04).

Langfeld, K, Graham, DI, Greaves, DM, Mehmood, A, Reis, T, (2016). "The Virtual Source Approach to Non-Linear Potential Flow Simulation," Proc 26th Int Offshore and Polar Eng Conf, Rhodes, Greece, 26 June-2 July, 2016.

Longuet-Higgins, M, and Cokelet, E (1976). "The Deformation of Steep Surface Waves on Water. I. A Numerical Method of Computation," Proceedings of the Royal Society of London. Series A, Mathematical and Physical Sciences, 350(1660), 1-26.

Qian, L., Causon, D. M., Mingham, C. G. and Ingram, D. M. (2006), A free-surface capturing method for two fluid flows with moving bodies, in 'Proc. R. Soc. A', Vol. 462, The Royal Society, pp. 21–42.

Smith, I, Griffiths, D, and Margetts, L (2014). "Programming the Finite Element Method," Wiley, 2014.

Thomas, T.J. and Dwarakish, G.S., 2015. Numerical wave modelling–A review. Aquatic Procedia, 4, pp.443-448.